Hairpin Folding Dynamics: The Cold-Denatured State Is Predisposed for Rapid Refolding†

R. Brian Dyer,*,‡ Shelia J. Maness,§ Stefan Franzen,§ R. Matthew Fesinmeyer,|| Katherine A. Olsen,|| and Niels H. Andersen*,||

Bioscience Division, Mail Stop J586, Los Alamos National Laboratory, Los Alamos, New Mexico 87545, Chemistry Department, North Carolina State University, Raleigh, North Carolina 27695, and Chemistry Department, University of Washington, Seattle, Washington 98195

Received April 15, 2005; Revised Manuscript Received June 3, 2005

ABSTRACT: Cold denaturation is a general phenomenon in globular proteins, and the associated cold-denatured states of proteins have important fundamental and practical significance. Here, we have characterized the cold-denatured state of a β-hairpin forming peptide, MrH3a, in 8% hexafluoro-2-propanol (HFIP) and the dynamics of its refolding following a laser-induced T-jump. β-Hairpins constitute an important class of protein structural elements, yet their folding mechanisms are not fully understood. Characterization of MrH3a using NMR, CD, and IR spectroscopies reveals residual structure in the cold-denatured state, in contrast with the highly disordered heat-denatured state. The residual structure in the cold-denatured state comprises relatively compact and solvent protected conformations. Furthermore, we find a substantial acceleration in the rate of folding from the cold-denatured state compared to that of the heat-denatured state. In addition, the cold-denatured state is not populated in 20% HFIP; folding occurs only from the fully unfolded state and is significantly slower. We interpret the acceleration of the folding rate of MrH3a in 8% HFIP as a direct consequence of the collapsed conformations of the cold-denatured state. Finally, there may be some reduction of the loop search cost when starting from the cold-denatured state, since this state may have some of the stabilizing cross-strand interactions already formed.

Cold denaturation is a general phenomenon in globular proteins, and the associated cold-denatured states of proteins have important fundamental and practical significance. The residual structures of cold-denatured proteins have been characterized and found to be comparable to the structures of folding intermediates in several cases, including barstar (*1*), β-lactoglobulin (*2*), lysozyme (*3*), and ribonuclease A (*4*). This observation has led to the hypothesis that residual structures in the cold-denatured state represent initiation sites for refolding. Cold-denatured states also have a practical significance for the study of the early events in protein folding: they can be exploited as a means to rapidly refold a protein using a laser-induced temperature jump (*5*−*7*). Despite the importance of cold-denatured states of proteins, relatively little is known about how such states compare with other unfolded states (produced either by heat or a chemical denaturant) and how the refolding dynamics might differ, depending on the starting state.

Peptide models are valuable experimental systems for studying the fundamental processes of protein folding (*8*−*10*). Many essential processes have been observed in the folding of peptide models, including secondary structure formation, hydrophobic collapse, hydrogen bond formation, and side-chain packing (*11*−*14*). Andersen has demonstrated that small peptides that adopt specific secondary structures can also be induced to unfold at low temperatures (*15*, *16*). This opens the possibility for studying fast events in the refolding of such peptide models of secondary structure motifs using laser-induced T-jumps.[1] Using this approach, we demonstrated that helix formation from completely unfolded conformations (thus requiring helix nucleation) is a fast, sub-microsecond process (*17*). Here, we have characterized the cold-denatured state of a β-hairpin-forming peptide and the dynamics of its refolding following a laser-induced T-jump.

β-Hairpins constitute an important class of protein structural elements. Recent advances in the design of stable, soluble peptides with β-turn and β-sheet structures (*18*−*25*) have led to improved understanding of the stability and folding dynamics of such structures. T-jump relaxation dynamics of a number of β-hairpin peptides have been reported, including the 16-residue C-terminal β-hairpin fragment of protein G (GB1, (*26*)), cyclic gramicidin analogues (*27*), and a de novo designed hairpin (HP1) (*28*). We have explored the role of the loop search necessary to form the stabilizing cross-strand interactions in linear peptides that form β-hairpin structures; our system employed a stabilizing hydrophobic cluster connected by loops of dif-

† This research was supported by National Institutes of Health Grants GM53640 (R.B.D.) and GM59658 (N.H.A.) and by National Science Foundation Grant CHE0315361 (N.H.A.).

* To whom correspondence should be addressed. Phone, (505) 667-4194; fax, (505) 667-0851; e-mail: bdyer@lanl.gov (for R.B.D.). Phone, (206) 543-7099; e-mail, andersen@chem.washington.edu (for N.H.A.).

‡ Los Alamos National Laboratory.

§ North Carolina State University.

|| University of Washington.

[1] Abbreviations: T-jump, temperature jump; FTIR, Fourier transform infrared; HFIP, hexafluoro-2-propanol; TFA, trifluoroacetate; SVD, singular value decomposition; CSD, chemical shift deviation.

10.1021/bi050698z CCC: $30.25
Published on Web 07/06/2005

fering lengths (*29*). We found that the entropic cost of the loop search contributes to the transition state barrier and that the folding rate is accelerated by minimizing the loop search. These studies employed 21 vol % hexafluoro-2-propanol (HFIP) as the solvent, since the shorter hairpin sequence was not well-populated without the addition of fluoroalcohol cosolvents.

Cold denaturation has now been observed for more than 10 peptide hairpins (*16*, *19*, *21*, *24*, *30*−*33*). The first observations were made in water and 20 vol % methanol by the Searle group for a peptide (MrH1) designed to mimic the two-stranded, antiparallel, DNA-binding β-sheet motif of the *met* repressor. We demonstrated that the tendency toward cold-denaturation was enhanced in 8−10 vol % HFIP (*16*). Folding studies of MrH1 are complicated by competing β-aggregate formation (*34*). Two close analogues were prepared, MrH3a and MrH4a (below), displaying a significantly reduced tendency to aggregate.

MrH1	KKYTVS-INGK-KITVSI (peptide H1 of ref *30*)
MrH3a	KKYTVS-INGK-KITVSA
MrH4a	KKLTVS-INGK-KITVSA
MrH3b	KKYTVS-I**p**GK-KITVSA
MrH4b	KKLTVS-I**p**GK-KITVSA

The peptides with an NG turn locus display a type I′ β-turn in the hairpin state, which is populated to different extents depending on the solvent composition and pH (*35*). In analogy to Gellman's studies of similar hairpin sequences (*36*, *37*), the replacement of the NG turn locus with a D-Pro−Gly unit (**p**G) increases the hairpin fold population and provides systems that are nearly 100% folded. These serve as calibration points for the use of strand resonance chemical shift measures of fold population.

Peptides MrH3a and MrH4a retain the cold-denaturing feature first observed for MrH1. To delimit the structural hypotheses appropriate for cold-denaturing hairpins of this series, the structural features of MrH3a and MrH4a evidenced by CD, IR, and NMR spectroscopy over a range of temperatures and solvent compositions have been determined. The NMR parameters are residue-specific measures of structuring and thus provide a means for determining whether some, but not all, of the structural preferences of these peptides are retained under conditions of incomplete folding. Furthermore, the refolding dynamics of MrH3a following a T-jump are far more complex than reported previously (*29*) in the absence of cold-denaturation. Our results demonstrate that the cold- and heat-denatured states are substantially different and that the folding/unfolding dynamics are highly dependent on the initial state.

MATERIALS AND METHODS

Peptides. Hairpin peptides were synthesized using FMOC chemistry on an Applied Biosystems 433A synthesizer. The MrH3a sequence is a modification (a C-terminal I to A substitution to improve solubility) of a previously reported sequence (*16*, *30*). The C-terminal I to A substitution in MrH3a improves the peptide solubility and reduces its tendency toward β-aggregate formation. The peptides were purified by reverse-phase HPLC (C18 column) using a water/acetonitrile gradient. For the IR studies, the peptides were deuterium-exchanged by repeated lyophilization from D_2O. Trifluoroacetic acid (TFA), which was used in the HPLC purification, was present as an impurity in all samples. Samples were dissolved in solutions ranging from 4 to 21 vol % hexafluoro-2-propanol (HFIP) in D_2O (99.9%, Sigma) with no added buffer, and final concentrations for the IR studies were determined to be in the range of 1−4 mM as determined by the UV absorption of Tyr at 274 nm.

NMR Melting Studies. All NMR experiments were performed using a Bruker DRX-500 spectrometer. A combination of TOCSY (60 ms MLEV-17 spinlock) and NOESY (150 ms mixing time) 2D NMR spectra was used to assign all resonances. The samples consisted of ~2 mM peptide in phosphate-buffered water at pH 6 with 10% D_2O. Some samples used deuterated trifluoroethanol (TFE) or hexafluoro-2-propanol (HFIP) as cosolvents, which were added in the appropriate amounts by gastight syringe. Sodium 2,2-dimethyl-2-silapentane-5-sulfonate (DSS) was used as the internal chemical shift reference and set to 0 ppm for all conditions independent of temperature, pH, and cosolvent concentration.

NMR fraction-folded measures based on the difference in chemical shift of the Gly9 alpha protons were calculated as $\delta H\alpha_{downfield} - \delta H\alpha_{upfield}$. The difference values were converted to fraction-folded values using a linear scale, for which a difference of 0 ppm was considered to represent the fully unfolded state and a difference of 0.707 ppm was taken to represent 100% folded. The latter was an extrapolation based on the observation of a 0.622 ppm difference for MrH3a in 30% TFE at 280 K, conditions under which the peptide was considered to be 88% folded based on strand shift comparison with MrH3b in 30% TFE (see immediately below).

Strand-based measures were derived from the sum of the CSDs of inwardly directed Hα protons located near the hairpin core (positions S $\pm$ 2,4). The deviations were determined using a calculation and analysis application developed in the Andersen lab, *CSDb* (*19*) (available at http://andersenlab.chem.washington.edu), capable of correcting for cosolvent, temperature, pH, nearest-neighbor, and end-related effects. A sum of 0 ppm was considered to represent 0% folded, and a sum of 3.516 ppm was taken as 100% folded. As with the turn-measure, the 100%-fold point represents an extrapolation from other data; in this case, the most-folded value for MrH3b, in 30% TFE at 280 K, provided a value of 3.375 ppm; these conditions are believe to provide a 96%-structured ensemble based on a fit to the NMR melting curve.

CD Melting Studies. Circular dichroism stock solutions are prepared by dissolving weighed amounts of peptides in 20 mM aqueous, pH 6, phosphate buffer to make a solution of about 500 μM. The concentration of stock solutions is measured by the UV absorption of tyrosine ($\epsilon = 1420\ M^{-1}\ cm^{-1}$ at 276 nm). CD samples were diluted appropriately to obtain 30 μM solutions of the peptide in buffer. Fluoroalcohols were added in the appropriate amounts as needed using gastight microsyringes.

Spectra were recorded on a Jasco J715 spectropolarimeter using 0.10 cm path length cells. The calibration of the wavelength and degree ellipticity scales has been described previously (*38*, *39*). Spectral accumulation parameters were usually a scan rate of 100 nm/min, a 0.2 nm step resolution over the range of 190−270 nm with 16 scans averaged for

each spectrum. The accumulated average spectra were trimmed at a dynode voltage of 600 V prior to blank subtraction and smoothing, which used the reverse Fourier transform procedure in the Jasco spectra analysis software. For melting experiments, the temperature was increased from 5 to 95 °C in 10 °C increments. Each step was equilibrated at the target temperature for 5 min before acquiring data. CD data for MrH3a and MrH3b are reported in residue-molar ellipticity units (deg cm^2 residue-dmol^{-1}), and for MrH4a are reported in millidegrees ellipticity due to the lack of an aromatic residue for precise concentration determination. The CD monitored melting studies are reported as $[\theta]_{max} - [\theta]_{min}$ versus temperature. The $[\theta]_{max}$ is the value at the maximum if one is observed in the 195−202 nm range or the most positive value observed between 198 and 203 nm.The $[\theta]_{min}$ is the value at the minimum if one is observed in the 213−219 nm range or the most negative value between 214 and 218 nm. This measure, as $[\theta]_{198} - [\theta]_{214}$, is negative ($< -20\,000$ deg cm^2 residue-dmol^{-1}) for the statistical coil state (*16*).

Infrared Spectroscopy. The equilibrium melting behavior of the hairpin peptides was studied using FTIR spectroscopy. FTIR spectra were collected on a Bio-Rad FTS-40 interferometer using a temperature-controlled IR cell. The IR cell contained both the sample and a D_2O reference solution between CaF_2 windows with a 100 μm spacer. The cell is translated laterally under computer control to acquire matching sample and reference single beam spectra, and the protein absorption spectrum is computed as $-\log(I_{samp}/I_{ref})$.

T-Jump Relaxation Measurements. The T-jump relaxation apparatus has been described previously (*40*). Briefly, a laser-induced T-jump is used to rapidly shift the folding/unfolding equilibrium, and the relaxation kinetics are measured using time-resolved infrared spectroscopy. The T-jump perturbation generated by a laser heating pulse is faster than the molecular dynamics of interest. The T-jump pulse is generated by Raman-shifting a Q-switched Nd:YAG (Spectra Physics DCR-4) fundamental at 1064 nm in H_2 gas (1-Stokes shift), producing a 10 ns pulse at 1.91 μm. The near-infrared wavelength is partially absorbed by the D_2O ($\epsilon \sim 6$ cm^{-1}, or 87% transmittance in a 100 μm path length cell), and the absorbed energy is rapidly thermalized within the irradiated volume. The magnitude of the T-jump produced depends on the per pulse energy and the focus of the laser, typically 40 mJ and 1 mm spot diameter respectively, which yields an 11 °C T-jump. The mid-IR probe beam is a continuous wave lead−salt diode laser (Laser Photonics) with a tunable output range of 1600−1700 cm^{-1}. The probe beam is focused to a 50 μm (1/e^2 diameter) spot at the center of the heated volume. Probing only the center of the heated volume ensures a uniform temperature distribution in the probe volume by avoiding the temperature gradient produced on the wings of the Gaussian pump beam (*41*). The transient transmission of the probe beam through the sample is measured using a fast (100 MHz) photovoltaic MCT IR detector/preamplifier (Kolmar Technologies). Transient signals are digitized, and the signal is averaged using a Tektronics digitizer (7612D). Instrument control and data collection are accomplished using a LabVIEW computer program. Measurements of the transient absorbance for both the sample and the reference were collected from 10^{-9} to 10^{-1} s, and relaxation times were obtained using a deconvolution process described below.

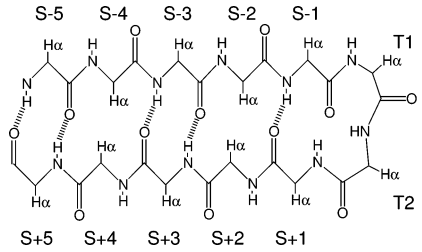

FIGURE 1: Structural features and residue nomenclature for [2:2] hairpins.

Analysis of Kinetics Data. Accurate determination of the peptide relaxation kinetics requires deconvolution of the instrument response function from the observed kinetics. Very accurate deconvolution of the instrument response is possible because it is determined concurrently with each sample measurement under the exact same conditions. The instrument response function for the system is taken to be the derivative of the reference trace, normalized to have an integral of 1 at the maximum of the reference trace. The decay function used is an exponential decay with the formula (A·exp($-kT$)), where A and k are the change in absorbance and the rate, respectively. The reported relaxation rates represent an average of at least four separate trials.

RESULTS

Fold Populations and Equilibrium Characterization of Cold- and Heat-Denatured States of Mr3Ha. There are a number of structural features in a [2:2]-hairpin state that give rise to diagnostic spectroscopic signatures. The antiparallel alignment of numerous amide planes produces a CD signature consisting of a minimum at 215−218 nm and a maximum at 198−205 nm (*16*, *42*). Cross-strand hydrogen-bonding interactions between pairs of amides (notably S ± 3 and S ± 5, see Figure 1) (*16*, *21*, *33*, *43*, *44*) are observed as downfield H_N shift deviations. Close spatial interactions between alpha methines in the non-H-bonded strand resonances (S ± 2, S ± 4, etc.) also place these hydrogens in the deshielding region of both same- and cross-strand amide planes (*16*, *45*), and large phi/psi order parameters at residues S − 1 through S + 1 are associated with specific turn geometries that facilitate strand alignment.

On the basis of these features, a number of spectroscopic measures of hairpin population have been used in prior studies. Both the molar ellipticity of the ca. 216 nm CD minimum (*30*, *46*−*49*) and the amplitude of the couplet ($[\theta]_{max} - [\theta]_{min}$) (*16*, *50*) have been employed to monitor thermal and mutational effects on hairpin stability, but neither is readily converted into a direct measure of folded fraction. There has been greater success in calibrating NMR chemical shift measures of folding; the four approaches that have been used are listed here. (1) The CSDs of the inwardly directed Hα resonances (individually or summed) (*16*, *19*, *21*, *31*, *51*) appear to be the most sensitive measure. (2) More recently, (*19*, *31*) we added the CSDs of the H_Ns, but these are not as useful for melting studies due to the structure-dependent intrinsic temperature gradients of NH signals (*52*). (3) In systems with Gly as residue T2, the chemical shift difference between its diastereotopic Hα protons has been used to measure both hairpin population (*24*, *32*, *33*, *47*, *49*) and as a potential measure of the presence of turn formation in the absence of strand alignment (*21*). The Gly−CH_2

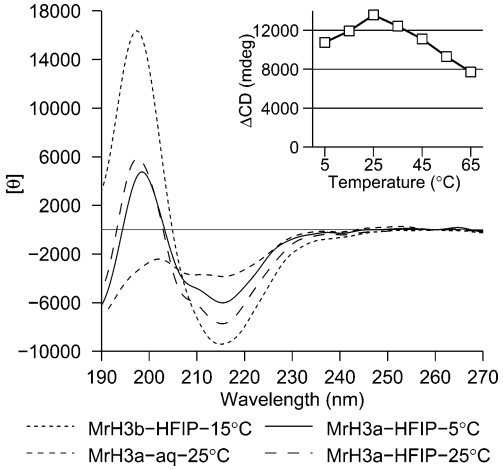

FIGURE 2: Representative CD spectra illustrate the characteristic β-hairpin signature for the MrH series of peptides. The inset displays the difference between the maximum and minimum spectral features ($[\theta]_{max} - [\theta]_{min}$), see Materials and Methods, over a range of temperatures for MrH3a in 8% HFIP. Even the system with least populated hairpin, MHr3a at 25 °C in water, represents a significant hairpin population: $[\theta]_{198}$ is significantly more negative than $[\theta]_{214}$ for an unfolded coil state.

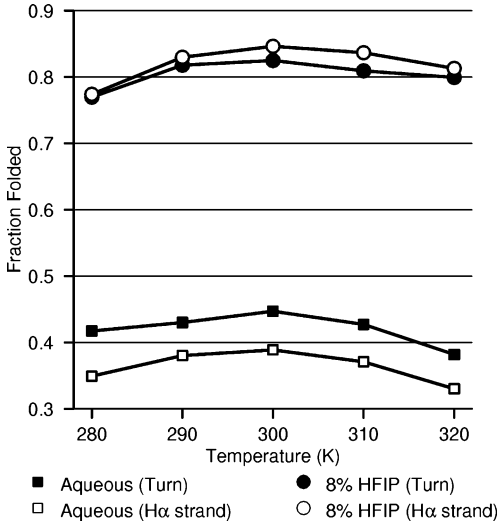

FIGURE 3: NMR measures of folding for MrH3a in aqueous and HFIP-containing solvents. The calibration procedure appears in Materials and Methods.

diastereotopicity measure may not be applicable for **p**G turns. In contrast, NMR measures 1 and 2 can be calibrated and expectation values for 100% folded are about the same, regardless of turn type. (4) The smaller downfield shifts (relative to the inward Hα at the non-H-bonded sites) of the Hα resonances of the S ± 1 and S ± 3 residues have also been used extensively (*11*, *14*, *53*, *54*), but there is no theoretical basis for calibration, and in the present case, these shifts are small and thus subject to greater experimental error.

Our interest here is focused on the thermal behavior of MrH3a in 8% HFIP, the medium in which we observed unusual initial-state-dependent relaxation kinetics. The general usefulness of the $[\theta]_{max} - [\theta]_{min}$ CD measure is illustrated in Figure 2. Solvent and mutation (an N → **p** mutation to position T2) effects establish that this measure does reflect hairpin population. The inset panel in Figure 2 provides clear evidence that either the fold population (or the ordering of the strand amide groups) in 8% HFIP decreases upon cooling.

Residue-specific NMR data have the potential to define the extent to which a folding transition is strictly two-state. If the equilibrium is, effectively, between a statistical coil state and a fully hairpin-like folded state, then all chemical shift measures of structuring should display the same solvent, mutation, and temperature dependence. For MrH3a and MrH3b in a variety of media (water at two pH's, 8% HFIP, and 30% TFE), this was the case for all three NMR measures mentioned above (data not shown). For conversion to folded fraction, we have assumed that MrH3b is 96% folded in 30% TFE at 280 K. Figure 3 shows the fraction-folded versus *T* data in 8% HFIP derived using the strand alignment specific measure (the sum of the Hα structuring shifts for T4, S6, K11, and T13) and the diastereotopic shift difference for the Gly^9-CH_2. Both measures show structure loss upon both cooling and warming with maximal structuring at ca. 295 K. These measures are concordant with the CD measure in Figure 2.

Qualitatively, the differences in structure as measured by the turn and strand probes are insignificant: the overall shape of the melting curve is in agreement. While there is some difference in the folded-fraction measure obtained from either the turn or strand probes in the case of strictly aqueous medium, in 8% HFIP this difference is largely absent. Both measures reveal cold denaturation. The extent of unfolding (i.e., loss of structuring chemical shifts) upon both warming and cooling from the maximum at 295 K is somewhat less using the turn measure. While this might be taken as an indication of some retained turn structure as the hairpin strand alignment is reduced at both high and low temperatures, studies with an analogue, the MrH4a sequence (vide infra), in which the extent of cold-induced unfolding is enhanced do not support this view.

Scheme 1

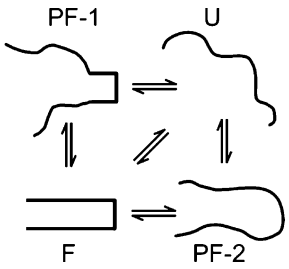

For MrH3a, the extent of unfolding observed upon cooling is quite small and the chemical shift and CD changes can all be rationalized within the context of the folding scheme shown (Scheme 1). Two-state folding would imply only the U and F states shown. The partially folded states, PF-1 and PF-2 represent species that could also be populated under conditions where the fully folded population is decreased. PF-1 represents conformers in which a fully formed turn at the native locus is present; this is a folding intermediate in the Muñoz−Eaton folding pathway (*26*). We hypothesize that PF-2, an alternative folding intermediate, is a contributor to the ensemble of unfolded states that form as a result of cold-denaturation. Its looser cross-strand hydrophobic cluster is reasonable given the decreased hydrophobic pressure toward compaction at lower temperatures. The U and both PF states would lack the CD signature of a hairpin, but PF-1 should retain the diastereotopic shift difference for Gly^9-

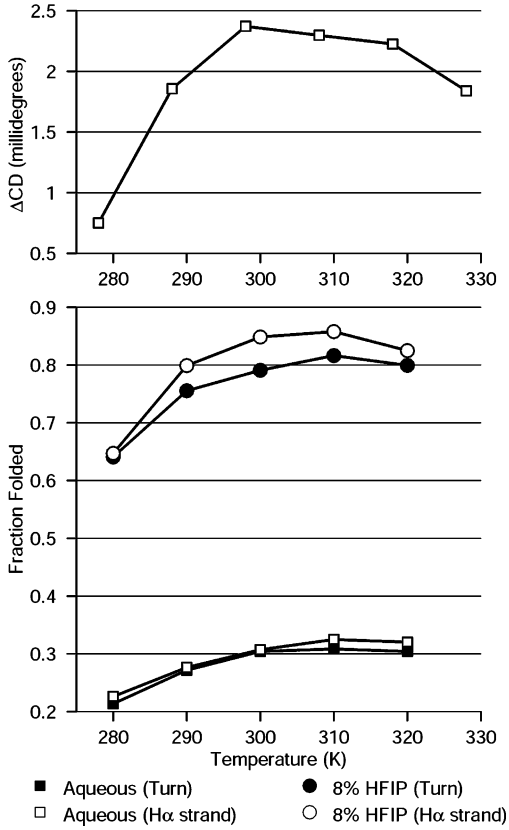

FIGURE 4: CD and NMR measures of fold for MrH4a. The top panel tracks the $([\theta]_{197} - [\theta]_{215})$ measure of β-hairpin structure (in millidegrees) for MrH4a in 8% HFIP. The expectation value for this $\Delta[\theta]$ measure for a coil state is ca. -1.8 mdeg at 5 °C. The lower panel employs turn and strand NMR probes to derive the temperature dependence of the folded fraction in both water and 8% HFIP. All measures indicate a significantly greater loss of structure is present due to cold denaturation than was observed for MrH3a.

CH_2. On the basis of the NMR data, the structured turn form (PF-1) cannot be the major "unfolded" species upon cooling.

Comparisons with an Analogue That Displays Enhanced Cold-Denaturation. Peptides MrH4a and MrH4b became available only after the T-jump studies on MrH3a were completed. The Y3L mutation destabilized the hairpin fold and increased the degree of cold-denaturation observed by all spectroscopic measures. Assuming that the folding equilibria of MrH3a and MrH4a are similar, MrH4a provides greater access to partially structured species that contribute to the cold- versus heat-denatured state. Spectroscopic data for MrH4a, analogous to that in Figure 3, appears in Figure 4.

The greater extent of structure loss upon cooling in the MrH4a analogue provides a clearer picture of the nature of the cold-denatured state. We observe that the order in the turn is lost to essentially the same extent as strand alignment, additional evidence that cold denaturation does not increase the population of PF-1. Further evidence for the lack of the PF-1 species in hairpin peptide equilibria under partially folded conditions comes from plots of fraction-folded data based on strand probes versus that from turn probes. When data for MrH3a and MrH4a in Figures 3 and 4B (as well as comparable data for these peptides in 30% TFE at 280 and 320 K, the former representing the most folded conditions for both peptides) are plotted as fraction-folded based on

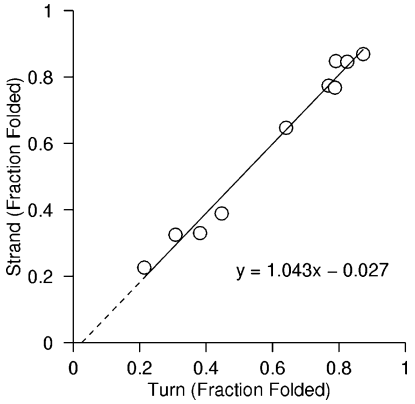

FIGURE 5: A comparison of turn ($\Delta\delta$-CH_2 for Gly^9) and cross-strand interaction NMR measures of folded population at conditions providing a range of percent-folded values. Measures for MrH3a and MrH4a in water, 8% HFIP, and 30% TFE at a variety of temperatures in the 280−320 K range are included. Extrapolation to zero strand alignment indicates that the turn content of the unfolded state is less than 10%.

the sum of the strand residue Hα sites versus the diastereotopic shift difference for the Gly^9-CH_2 measure (Figure 5), the slope of the well-correlated data ($R^2 = 0.98$) is 1.04. The correlation passes very close to the origin, specifically 0.03 fractional turn at zero strand alignment: the diastereotopic shift difference for Gly^9-CH_2 is thus an excellent measure of the population of the fully folded hairpin state.

Infrared Spectroscopic Measures of Folding in 8% HFIP. NMR and CD methods are useful for characterizing the equilibrium structures and populations of the β-hairpin, but neither can follow the fast folding/unfolding kinetics. Most previous studies of hairpin folding dynamics have been based on IR detection of the structural changes following a laser T-jump. Gai and co-workers (*28*) used the sharp, but weak, band at 1681 cm^{-1} to measure hairpin populations and the correlated, more intense, but broad, band at 1632 cm^{-1} to monitor changes after T-jumps; the two bands are attributed to in- and out-of-phase, inter-strand, dipole coupling among amide carbonyls associated with a β-sheet conformation. The same group (*55*) has monitored the kinetics of a trpzip hairpin at 1624 cm^{-1}. In a preliminary study (*35*) of MrH1 over the cold-denaturation limb, the largest changes in absorbance were observed at 1618 cm^{-1}. The T-jump kinetics of MrH3a in 21% HFIP were monitored at 1632 cm^{-1} (*29*). These studies demonstrate the utility of infrared spectroscopy for following the folding dynamics of β-hairpin structures.

The FTIR spectrum of MrH3a in 8% HFIP provides clear evidence for the formation of a stable β-hairpin structure. Three low-frequency components of amide I′ are observed in the second derivative spectrum (1628, 1634, and 1645 cm^{-1}; data not shown) at 25 °C. These three components of the amide I′ band, assigned to a β-turn and the inward and outward directed C═O groups of the β-sheet, that is, intra- and intermolecular (to water) hydrogen bonding, respectively (*27*), can be used to follow the temperature-dependent population of the β-hairpin structure. The temperature-dependent FTIR difference spectra for MrH3a in 8% HFIP in the amide I region are shown in Figure 6, along with the fraction-folded versus *T* data (inset). These difference spectra are generated using the spectrum at 25 °C as the reference spectrum and subtracting the spectrum at temperature *T* from that at 25 °C for $T < 25$ ($25 - T$; Figure 6, upper panel)

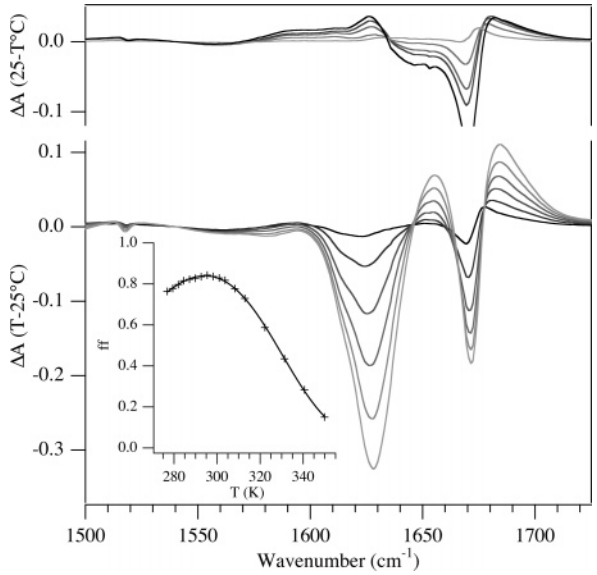

FIGURE 6: FTIR difference spectra for MrH3a in 8% HFIP. Upper panel, cold-denaturation limb (25 − T); lower panel, heat-denaturation limb (T − 25); inset, melt-curve monitored at 1626 cm^{-1}.

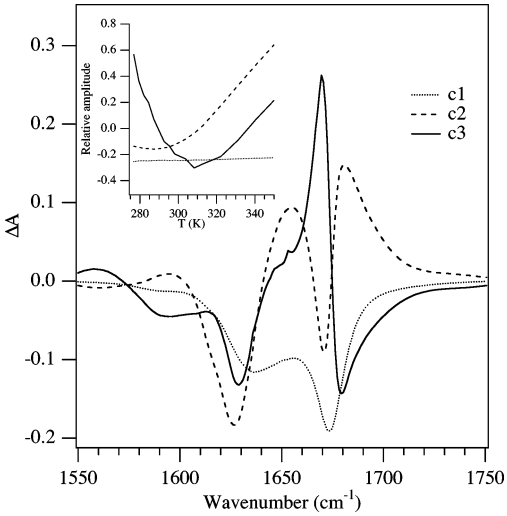

FIGURE 7: SVD analysis of *T*-dependent FTIR spectra of MrH3a. the first three principle components are plotted, and the temperature dependence of the amplitude of each component is plotted in the inset, with the corresponding line type.

and the inverse for $T > 25$ ($T - 25$; Figure 6, lower panel). The spectrum at 25 °C is near the maximum of the melt curve (inset) and thus is the best representation of the fully folded spectrum (although the folded fraction is still only 0.85 based on the NMR analysis). The difference spectra exhibit spectral changes associated with the loss of folded population as the temperature is raised or lowered from 25 °C. They also contain a derivative-shaped feature centered at 1672 cm^{-1} that is due to the temperature-dependent shift of the C═O stretch frequency of incompletely removed TFA from the HPLC purification. While this feature obscures part of the amide I region, the features characteristic of the hairpin structure are clearly discernible. The IR melt obtained by monitoring the IR absorbance at 1626 cm^{-1}, near the peak of the maximum difference feature, is shown in the inset. The folded fraction has been approximated by setting the maximum to 0.85, the value determined from the NMR analyses (Figure 3) and fitting the heat-denaturation branch to a 2-state model. The cold denaturation transition is clearly observed with approximately the same fraction of unfolding as observed in the NMR. The folded fraction estimated from the IR melt agrees well with the NMR determination over the entire range of the NMR measurements. Clearly, the difference feature centered near 1626 cm^{-1} is a sensitive measure of the hairpin population and can be used in T-jump measurements to follow the dynamics of the folded structure.

The MrH3a FTIR difference spectra over the cold- and warm-limbs of the melt are clearly different. First, the isosbestic point shifts from 1634 to 1646 cm^{-1} for the low- and high-temperature transitions, respectively. As the temperature is increased from 4 to 25 °C, the features associated with the β-hairpin structure grow in intensity (Figure 6, upper panel). In contrast, as the temperature is further increased from 25 to 77 °C, these features decrease in intensity (Figure 6, lower panel). The feature centered at 1626 cm^{-1} is broader and displays a shoulder at ca. 1615 cm^{-1} over the heat-denaturing limb. There are also differences in the region (1650−1660 cm^{-1}) where the statistical coil band is expected. The population of at least three different states (folded, unfolded, and partially folded or cold-unfolded states) is required to account for the evolution of the difference spectrum from low to high temperature. These observations suggest that the β-hairpin structure is only partially disrupted in the cold-denatured state, although they do not reveal the exact nature of the residual structure.

An SVD analysis of the temperature dependence of the FTIR spectra provides a clearer picture of the distinction between the cold-denaturing and heat-denaturing transitions than the difference spectra alone. The results of this SVD analysis are shown in Figure 7. Two components capture nearly 90% of the variance in the temperature-dependent FTIR spectra. A third component (c1) is essentially invariant over the whole temperature range studied, with the spectral shape similar to the amide I envelope. The remaining components (not shown) have small amplitudes and represent the noise in the data. The two temperature-dependent components provide a clearer picture of the distinction between the cold-denaturing and heat-denaturing transitions. The temperature dependence of these two components appears in the inset of Figure 7. Component c3 (the one with smallest amplitude) captures the changes associated with cold-denaturation. It has the sharp 1628 cm^{-1} feature and only a modest positive feature at 1650−1655 cm^{-1}, similar to what is observed in the low-temperature difference spectra of Figure 6. The dominant amplitude change for the c2 component occurs in the high-temperature region, and its spectral signature corresponds reasonably well to the difference spectra for the high-temperature transition of Figure 6. The notable features are the broader ca. 1628 cm^{-1} peak and a readily detected peak corresponding to an increase in the population of the fully unfolded coil state. The differences at 1655 cm^{-1} between c2 and c3 are more remarkable given that the strong feature appears in c2 where it would be most readily masked by the nearby negative peak due to TFA. In c3, this peak is a weak shoulder on the side of the TFA difference feature. Thus, the SVD analysis supports a 3-state model to describe the FTIR data, with distinct low- and high-temperature denatured states. Further, it appears that cold-denaturation does not produce coil spectral features in proportion to the loss of β-hairpin structure.

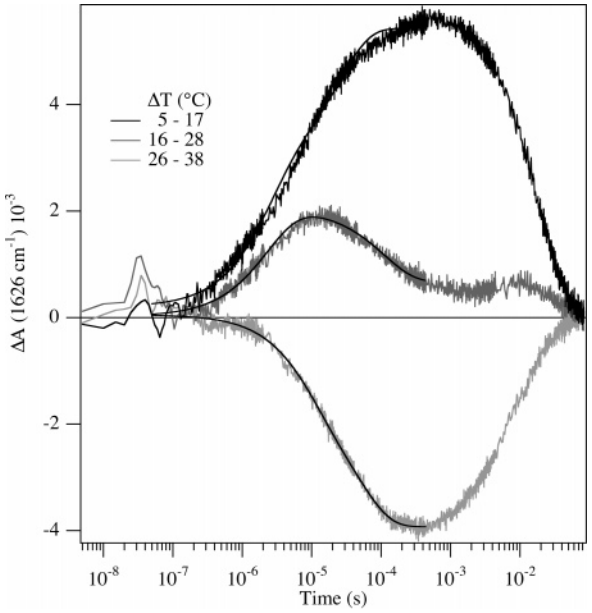

FIGURE 8: T-jump relaxation transients of MrH3a in 8% HFIP monitored in the amide I region (1626 cm^{-1}) following T-jumps over the ranges indicated in the legend.

Table 1: Relaxation Kinetics for MrH3a in 8% HFIP/D_2O

ΔT ($T_i - T_f$)/°C	amplitude/mOD	relaxation lifetime ($1/k_{rel}$)/μs
5−17	0.003	2.3
	0.003	25
16−28	0.002	2.4
	−0.001	111
26−38	−0.002	9.0
	−0.002	50

Dynamics of Refolding of MrH3a from a Cold-Denatured State. Selected IR relaxation kinetic traces following a laser-induced T-jump are shown in Figure 8. The kinetics are monitored at 1626 cm^{-1}, a frequency that is sensitive to both the cold- and heat-denaturation transitions (Figure 6). Three different relaxation measurements are shown: one (5−17 °C) over the cold-denaturing limb, one strictly within the melting limb (26−38 °C), and one (16−38 °C) through the temperature of maximal folding. Two well-separated kinetics phases are observed for T-jumps over 10 different temperature ranges (including the three shown in Figure 8), and all data can be fitted by biexponential functions. For the three experiments illustrated in Figure 8, the relaxation amplitudes and lifetimes are given in Table 1. A striking feature of these relaxation transients is that both phases are positive for the low-temperature jump (net gain in folded population), negative for the high-temperature jump (net loss), and alternately positive and negative for the intermediate temperature jump (with little net change). The observed relaxation kinetics of MrH3a in 8% HFIP are in sharp contrast to the behavior we have reported previously for the same peptide in 21% HFIP (*29*). Under the latter conditions, the relaxation kinetics are always single exponential, regardless of starting and ending temperature. The essential difference between these two conditions is that the peptide does not cold-denature in 21% HFIP and the equilibrium transition, as well as the kinetics, is well-described by a two-state model. Thus, the complexity of the relaxation kinetics reported here is clearly related to the cold-denaturation transition.

A kinetics model with a minimum of three states is required to fit the observed relaxation data. We postulate a kinetics model involving U, F, and PF-2 (Scheme 1):

$$\text{PF-2} \leftrightarrows \text{F} \leftrightarrows \text{U}$$

The PF-2 $\leftrightarrows$ F equilibrium dominates the low-temperature transition, and the F $\leftrightarrows$ U equilibrium dominates the high-temperature transition. We rule out PF-1 (containing residual turn structure) in this scheme based on the NMR evidence that this state is not significantly populated in the equilibrium sense and the absence of any infrared evidence that such a state is transiently populated. A third equilibrium is possible in this scheme (between PF-2 and U), but only two relaxation rates are observed, so only the indicated equilibria are considered in our model. Quantitative modeling of the observed relaxation rates in terms of this model requires knowledge of the individual equilibrium constants. We have determined the temperature-dependent population of F, but without a clear spectral signature for the PF-2 species, it has not been possible to do the same for this species. Nevertheless, the model provides an important framework in which to understand the origin of the observed fast and slow relaxations. Both a fast and a slow phase are observed for all T-jumps, regardless of starting temperature, but the signs and amplitudes of each phase varies depending on the position within the two transitions. The key to assigning the origin of each phase is the relaxation data for a T-jump that carries the system from the low- to the high-temperature branch of the melt curve (i.e., $\Delta T = 16 - 28$ °C in Figure 8). The fast phase is positive (meaning the population of F is increasing), whereas the slow phase is negative (decreasing population of F). Therefore, we assign the fast process to the relaxation of the PF-2 $\leftrightarrows$ F equilibrium in our kinetics model, and the slow process to relaxation of the F $\leftrightarrows$ U equilibrium.

Additional support for these assignments is provided by the time-resolved spectra in Figure 9. These spectra are generated from individual relaxation transients obtained for each wavelength (two of which are shown in the inset), following a T-jump from 4 to 22 °C (within the low-temperature transition). Both the fast process (represented by the 5 μs spectrum) and the slow process (represented by the 100 μs spectrum) show similar spectral features. The positive lobe of the transient spectra represents the growth of folded structure. This growth occurs with approximately equal amplitude in both the slow and fast phases. The amplitude of each phase is quantified in the biexponential fit to the 1625 cm^{-1} transient (the positive transient in the inset), which yields roughly equal amplitudes for the two phases. The negative lobe of the transient spectra has a major contribution from U (although there may also be some contribution from PF-2), based on the difference spectra and SVD analysis. Therefore, this spectral feature should dominate the relaxation kinetics of the U $\leftrightarrows$ F equilibrium. The amplitude of the slow phase is 1.5 times that of the fast phase when monitored at 1651 cm^{-1}, near the peak of the disordered structure band (the negative transient in the inset). This observation supports the assignment of the slow phase to the relaxation of the U $\leftrightarrows$ F equilibrium.

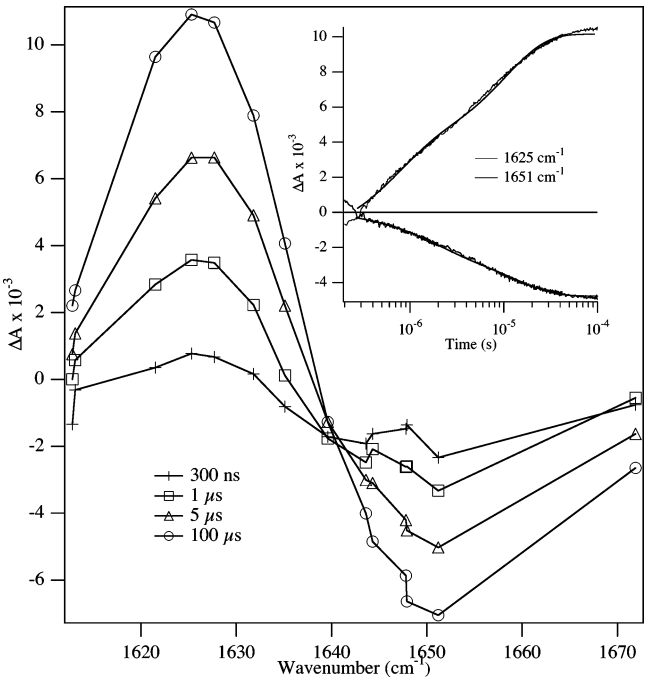

FIGURE 9: Time-resolved IR spectra following a T-jump from 4 to 20 °C (within the cold-denaturation branch). The relaxation transients at 1626 cm^{-1} (positive; gain of hairpin structure) and 1651 cm^{-1} (negative; loss of disordered structure) are shown in the inset, together with double exponential fits to the data.

DISCUSSION

Determining the effects of residual structure in denatured states of proteins on the kinetics and mechanism of folding is an area of active research. If such residual structure is native-like, it may serve to reduce the conformational space that must be searched and to nucleate the folding reaction, thus, speeding it up. Conversely, if the structure involves non-native interactions, it may be necessary to break up such interactions prior to productive folding, introducing an energy barrier to folding, thus, slowing it down. It is therefore important to determine both the nature of the residual structure and its effect on the folding kinetics to understand its influence on the folding mechanism. In the present study, we have found that the cold-denatured state of the β-hairpin-forming peptide MrH3a has residual structure, which has important implications for the refolding kinetics of this peptide.

Our results demonstrate that the cold-denatured state of MrH3a comprises relatively compact and solvent-protected conformations. First, the equilibrium FTIR and transient IR data provide clear evidence for differences in structure between the cold- and heat-denatured states of MrH3a. The heat-denatured state is highly disordered as evidenced by the strong, broad IR feature at 1655 cm^{-1} characteristic of the statistical-coil state. In contrast, the cold-denatured state exhibits this band only weakly and retains a sharp, low-frequency band with a characteristic frequency for a solvent-protected amide C═O stretch (1615 cm^{-1}). While the IR signature for this state is clearly different from the characteristic hairpin spectrum, at least some of the amide carbonyls must be buried and are likely involved in intramolecular H-bonding based on this very low amide I frequency. Further insight on the nature of the cold-denatured state is provided by the NMR data, which indicate a loss of the tight packing and H-bonding interactions that define both the turn and cross-strand interactions of the β-hairpin. Moreover, the NMR data rule out preferential loss of the sheet structure over the turn at low temperatures, and thus, PF-1 in the scheme is not significantly populated under these conditions. Taken together, these results support a model for the cold-denatured state as a collapsed state (PF-2), with some hydrophobic packing, but lacking the tight packing and the full complement of cross-strand H-bonds that define the hairpin fold.

Turning to the kinetics, two relaxation phases are observed in all T-jump data for MrH3a in 8% HFIP, in contrast to the strictly single-exponential kinetics observed under conditions for which there is no cold-denaturation (20% HFIP; (*29*)). We have modeled the 8% HFIP relaxation data with a 3-state equilibrium, including different cold- and heat-denatured states. The slowest relaxation rates occur for the F ⇆ U equilibrium probed on the heat-denaturation limb of the melt. We have previously shown that the unfolding rate of MrH3a in 20% HFIP is strongly temperature-dependent and slow ($1/k_u$ = 75 μs at 28 °C and 20 μs at 40 °C) (*29*). It is likely that the relaxation times of the slow phase are dominated by the unfolding rate, which accounts for the observed long relaxation times. In contrast, the fast phase within the cold-denaturation limb is likely dominated by the refolding rate from PF-2, at least at the lowest temperatures. The folding rate previously measured for MrH3a in 20% HFIP at 17 °C is 1/(6.8 μs) for U → F, compared to a folding rate of 1/(2.3 μs) for PF-2 → F. This represents an approximate 3-fold acceleration of the folding rate when starting from the cold-denatured state (PF-2) compared to the fully unfolded state (U). The same faster rate of folding is observed for the initial increase in hairpin population that occurs in a T-jump from the cold-denatured limb to the heat-denatured melting limb. Finally, the observation of differing folding rates from the cold- and heat-denatured states of MrH3a is in sharp contrast to the recent observation of indistinguishable folding rates from the cold- and heat-denatured states of the five-helix bundle protein λ_{6-85} (*59*). Since no apparent residual structure is present in the cold-denatured state of λ_{6-85}, this observation is further evidence that the rate acceleration for MrH3a is due to the presence of such structure.

The acceleration of the folding rate when starting from PF-2 is best understood in the context of other work on the mechanism of β-hairpin formation. Previously, we have investigated the folding mechanism of β-hairpin structures having a stabilizing hydrophobic cluster at different distances from the turn (*29*). Our results revealed a strong dependence of the folding rate on the length of the loop connecting the stabilizing, cross-strand interactions of the hydrophobic cluster. Furthermore, we found that the folding rate is accelerated in systems that are constrained to "collapsed" conformations. For example, the folding rates of a series of cyclic peptides that form stable β-hairpin structures are all about 10^7 s^{-1}, essentially the upper limit for β-hairpin formation (*27*). A related example is the folding of src SH3, for which insertion of a disulfide cross-link at the base of the distal β-hairpin increases the rate of folding of this protein 30-fold (*56*). The SH3 hairpin structure is likely formed in the transition state, and the transition state barrier (due in part to the loop entropy) is reduced by formation of the disulfide linkage. Theoretical simulations from the

Thirumalai group support these ideas. Simulation of the folding rate of a 16 residue, linear β-hairpin compared with the cyclic analogue (formed by cross-linking the C and N termini) predicts a 2.5-fold acceleration for the cyclic peptide (*57*). In addition, a greater than 2-fold increase was predicted for the rate of folding of the β-hairpin from Ig-binding protein when confined in an inert spherical pore (*58*). In light of these results, we interpret the acceleration of the folding rate of MrH3a in 8% HFIP as a direct consequence of the collapsed conformation of the cold-denatured state (PF-2). We present clear evidence that PF-2 is not a statistical coil state, but rather has some degree of compactness and solvent protection. In 20% HFIP, this state is not populated; folding occurs only from the fully unfolded state and is therefore slower. Finally, there may be some reduction of the loop search cost when starting from PF-2, since this state may have some of the stabilizing cross-strand interactions already formed.

Clearly, residual structure in the cold-denatured state of MrH3a speeds up the refolding reaction, possibly by reduction of the loop entropy and by facilitating the formation of the cross-strand H-bonds. An interesting question is whether the PF-2 state resembles the transition state for folding. While the compact topology and stabilizing cross-strand interactions present in PF-2 likely resemble the transition state, non-native interactions in PF-2 are also possible. Such non-native interactions would introduce additional barriers to folding that are not present in the transition state. Further characterization of the transition state and PF-2 structures will be necessary to resolve this issue.

REFERENCES

1. Wong, K. B., Freund, S. M., and Fersht, A. R. (1996) Cold denaturation of barstar, ^{1}H, ^{15}N and ^{13}C NMR assignment and characterization of residual structure, *J. Mol. Biol. 259*, 805−818.
2. Katou, H., Heshino, M., Kamikubo, H., Batt, C. A., and Goto, Y. (2001) Native-like β-hairpin retained in the cold-denatured state of β-lactoglobulin, *J. Mol. Biol. 310*, 371−484.
3. Nash, D., and Jonas, J. (1997) Structure of pressure-assisted, cold-denatured lysozyme and comparison with lysozyme folding intermediates, *Biochemistry 36*, 14375−14383.
4. Zhang, J., Peng, X., Jones, A., and Jonas, J. (1995) NMR study of the cold, heat and, pressure unfolding of ribonuclease A, *Biochemistry 34*, 8631−8641.
5. Nolting, B. (1996) Temperature-jump induced fast refolding of cold-unfolded protein, *Biochem. Biophys. Res. Commun. 227*, 903−908.
6. Ballew, R. M., Sabelko, J., and Gruebele, M. (1996) Direct observation of fast protein folding: the initial collapse of apomyoglobin, *Proc. Natl. Acad. Sci. U.S.A. 93*, 5759−5764.
7. Gilmanshin, R., Williams, S., Callender, R. H., Woodruff, W. H., and Dyer, R. B. (1997) Fast events in protein folding: relaxation dynamics of secondary and tertiary structure in native apomyoglobin, *Proc. Natl. Acad. Sci. U.S.A. 94*, 3709−3713.
8. Callender, R. H., Dyer, R. B., Gilmanshin, R., and Woodruff, W. H. (1998) Fast events in protein folding: the time evolution of primary processes, *Annu. Rev. Phys. Chem. 49*, 173−202.
9. Eaton, W. A., Munoz, V., Hagan, S. J., Jas, G. S., Lapidus, L. J., Henry, E. R., and Hofrichter, J. (2000) Fast kinetics and mechanisms in protein folding, *Annu. Rev. Biophys. Biomol. Struct. 29*, 327−359.
10. Kubelka, J., Hofrichter, J., and Eaton, W. A. (2004) The protein folding 'speed limit', *Curr. Opin. Struct. Biol. 14*, 76−88.
11. Espinosa, J. F., and Gellman, S. H. (2000) A designed beta-hairpin containing a natural hydrophobic cluster, *Angew. Chem., Int. Ed. 39*, 2330−2333.
12. Krantz, B. A., Moran, L. B., Kentsis, A., and Sosnick, T. R. (2000) D/H amide kinetic isotope effects reveal when hydrogen bonds form during protein folding, *Nat. Struct. Biol. 7*, 62−71.
13. Ramirez-Alvarado, M., Kortemme, T., Blanco, F. J., and Serrano, L. (1999) beta-Hairpin and beta-sheet formation in designed linear peptides, *Bioorg. Med. Chem. 7*, 93−103.
14. Syud, F. A., Stanger, H. E., and Gellman, S. H. (2001) Interstrand side chainEnDashEnDash−side chain interactions in a designed beta-hairpin: significance of both lateral and diagonal pairings, *J. Am. Chem. Soc. 123*, 8667−8677.
15. Andersen, N. H., Cort, J. R., Liu, Z., Sjoberg, S. J., and Tong, H. (1996) Cold denaturation of monomeric peptide helices, *J. Am. Chem. Soc. 118*, 10309−10310.
16. Andersen, N. H., Dyer, R. B., Fesinmeyer, R. M., Gai, F., Liu, Z. H., Neidigh, J. W., and Tong, H. (1999) Effect of hexafluoroisopropanol on the thermodynamics of peptide secondary structure formation, *J. Am. Chem. Soc. 121*, 9879−9880.
17. Werner, J. H., Dyer, R. B., Fesinmeyer, R. M., and Andersen, N. H. (2002) Dynamics of the primary processes of protein folding: helix nucleation, *J. Phys. Chem. B 106*, 487−494.
18. Cochran, A. G., Skelton, N. J., and Starovasnik, M. A. (2001) Tryptophan zippers: stable, monomeric β-hairpins, *Proc. Natl. Acad. Sci. U.S.A. 98*, 5578−5583.
19. Fesinmeyer, R. M., Hudson, F. M., and Andersen, N. H. (2004) Enhanced hairpin stability through loop design: the case of the protein G B1 hairpin, *J. Am. Chem. Soc. 126*, 7238−7243.
20. Gellman, S. H. (1998) Minimal model systems for beta sheet secondary structure in proteins, *Curr. Opin. Chem. Biol. 2*, 717−725.
21. Griffiths-Jones, S. R., Maynard, A. J., and Searle, M. S. (1999) Dissecting the stability of a β-hairpin peptide that folds in water: NMR and molecular dynamics analysis of the β-turn and β-strand contributions to folding, *J. Mol. Biol. 292*, 1051−1069.
22. Jäger, M., Nguyen, H., Crane, J. C., Kelly, J. W., and Gruebele, M. (2001) The folding mechanism of a β-sheet: the WW domain, *J. Mol. Biol. 311*, 373−393.
23. Schenck, H. L., and Gellman, S. H. (1998) Use of a designed triple-stranded antiparallel β-sheet to probe β-sheet cooperativity in aqueous solution, *J. Am. Chem. Soc. 120*, 4869−4870.
24. Searle, M. S. (2001) Peptide models of protein beta-sheets: design, folding and insights into stabilising weak interactions, *J. Chem. Soc., Perkin Trans. 2*, 1011−1020.
25. Smith, C. K., and Regan, L. (1997) Construction and design of β-sheets, *Acc. Chem. Res. 30*, 153−161.
26. Muñoz, V., Thompson, P. A., Hofrichter, J., and Eaton, W. A. (1997) Folding dynamics and mechanism of β-hairpin formation, *Nature 390*, 196−199.
27. Maness, S. J., Franzen, S., Gibbs, A. C., Causgrove, T. P., and Dyer, R. B. (2003) Nanosecond temperature jump relaxation dynamics of cyclic β-hairpin peptides, *Biophys. J. 84*, 3874−3882.
28. Xu, Y., Oyola, R., and Gai, F. (2003) Infrared study of the stability and folding kinetics of a 15-residue β-hairpin, *J. Am. Chem. Soc. 125*, 15388−15394.
29. Dyer, R. B., Maness, S. J., Peterson, E. S., Franzen, S., Fesinmeyer, R. M., and Andersen, N. H. (2004) The mechanism of β-hairpin formation, *Biochemistry 43*, 11560−11566.
30. Maynard, A. J., Sharman, G. J., and Searle, M. S. (1998) Origin of β-hairpin stability in solution: structural and thermodynamic analysis of the folding of a model peptide supports hydrophobic stabilization in water, *J. Am. Chem. Soc. 120*, 1996−2007.
31. Andersen, N. H., Fesinmeyer, R. M., and Hudson, F. M. (2004) Analysis of β-peptides using chemical shift deviations, in *Peptide Revolution: Genomics, Proteomics, and Therapeutics* (Charev, M., and Sawyer, T. K., Eds.) p 463, American Chemical Society, Washington, DC.
32. Kiehna, S. E., and Waters, M. L. (2003) Sequence dependence of β-hairpin structure: comparison of a salt bridge and an aromatic interaction, *Protein Sci. 12*, 2657−2667.
33. Tatko, C. D., and Waters, M. J. (2004) Comparison of C−H$\cdots\pi$ and hydrophobic interactions in a β-hairpin peptide: impact on stability and specificity, *J. Am. Chem. Soc. 126*, 2028−2034.
34. Colley, C. S., Griffiths-Jones, S. R., George, M. W., and Searle, M. S. (2000) Do interstrand hydrogen bonds contribute to β-hairpin peptide stability in solution? IR analysis of peptide folding in water, *Chem. Commun. 2000*, 593−594.
35. Andersen, N. H., Dyer, R. B., Fesinmeyer, R. M., Matthew, R., Gai, F., Maness, S. J., and Werner, J. H. (2001) Timescales for peptide secondary and tertiary structure formation, in *Peptides*

2000 (Martinez, J., and Fehrentz, J.-A., Eds.) pp 553−554, EDK, Paris, France.
36. Haque, T. S., and Gellman, S. (1997) Insights on β-hairpin stability in aqueous solution from peptides with enforced type I′ and type II′ β-turns, *J. Am. Chem. Soc. 119*, 2303−2304.
37. Syud, F. A., Espinosa, J. F., and Gellman, S. H. (1999) NMR-based quantification of β-sheet populations in aqueous solution through use of reference peptides for the folded and unfolded states, *J. Am. Chem. Soc. 121*, 11577−11578.
38. Andersen, N. H., Liu, Z., and Prickett, K. S. (1996) Efforts toward deriving the CD spectrum of a 3_{10} helix in aqueous medium, *FEBS Lett. 399*, 47−52.
39. Andersen, N. H., Brodsky, Y., Neidigh, J. W., and Prickett, K. S. (2002) Medium-dependence of the secondary structure of exendin-4 and glucagon-like-peptide-1, *Bioorg. Med. Chem. 10*, 79−85.
40. Williams, S., Causgrove, T. P., Gilmanshin, R., Fang, K. S., Callender, R. H., Woodruff, W. H., and Dyer, R. B. (1996) Fast events in protein folding: helix melting and formation in a small peptide, *Biochemistry 35*, 691−697.
41. Wray, W. O., Aida, T., and Dyer, R. B. (2002) Photoacoustic cavitation and heat transfer effects in the laser-induced temperature jump in water, *Appl. Phys. B 74*, 57−66.
42. Cort, J. R., Liu, Z., Lee, G. M., Harris, S. M., Prickett, K. S., Gaeta, L. S. L., and Andersen, N. H. (1994) β-Structure in human amylin and two designer β-peptides: CD and NMR spectroscopic comparisons suggest soluble β-oligomers and the absence of significant populations of β-strand dimers, *Biochem. Biophys. Res. Commun. 204*, 1088−1095.
43. Stanger, H. E., Syud, F. A., Espinosa, J. F., Giriat, I., Muir, T., and Gellman, S. H. (2001) Length-dependent stability and strand length limits in antiparallel β-sheet secondary structure. *Proc. Natl. Acad. Sci. U.S.A. 98*, 12015−12020.
44. Tatko, C. D., and Waters, M. L. (2003) The geometry and efficacy of cation-π interactions in a diagonal position of a designed β-hairpin. *Protein Sci. 12*, 2443−2452.
45. Sharman, G. J., Griffiths-Jones, S. R., Jourdan, M., and Searle, M. S. (2001) Effects of amino acid ϕ,ψ propensities and secondary structure interactions in modulating Hα chemical shifts in peptide and protein β-sheets, *J. Am. Chem. Soc. 123*, 12318−12324.
46. Ramírez-Alvarado, M., Blanco, F. J., and Serrano, L. (1996) De novo design and structural analysis of a model β-hairpin peptide system, *Nat. Struct. Biol. 3*, 604−612.
47. Griffiths-Jones, S. R., and Searle, M. S. (2000) Structure, folding, and energetics of cooperative interactions between the beta-strands of a de novo designed three-stranded antiparallel beta-sheet peptide, *J. Am. Chem. Soc. 122*, 8350−8356.
48. Ciani, B., Jourdan, M., and Searle, M. S. (2003) Stabilization of β-hairpin peptides by salt bridges: role of preorganization in the energetic contribution of weak interactions, *J. Am. Chem. Soc. 125*, 9038−9047.
49. Santiveri, C. M., Santoro, J., Rico, M., and Jiménez, M. A. (2004) Factors involved in the stability of isolated β-sheets: turn sequence, β-sheet twisting and hydrophobic surface burial, *Protein Sci. 13*, 1134−1147.
50. López de la Paz, M., Lacroix, E., Ramírez-Alvarado, M., and Serrano, L. (2001) De novo automatic design of β-sheet peptides, *J. Mol. Biol. 312*, 229−246.
51. Andersen, N. H., Barua, B., Fesinmeyer, R. M., Hudson, F. M., Lin, J., Euser, A., and White, G. (2002) Chemical shifts, the ultimate test of polypeptide folding cooperativity, in *Peptides 2002: Proc. 27th Eur. Peptide Symp.*, pp 824−825, Edizioni Ziino, Napoli and Sorrento, Italy.
52. Andersen, N. H., Neidigh, J. W., Harris, S. M., Lee, G. M., Liu, Z., and Tong, H. (1997) Extracting Information from the temperature gradients of polypeptide NH chemical shifts. 1. The importance of conformational averaging, *J. Am. Chem. Soc. 119*, 8547−8561.
53. Syud, F. A., Stanger, H. E., Mortell, H. S., Espinosa, J. F., Fisk, J. D., Fry, C. G., and Gellman, S. H. (2003) Influence of strand number on antiparallel β-sheet stability in designed three- and four-stranded β-Sheets, *J. Mol. Biol. 326*, 553−568.
54. Espinosa, J. F., Syud, F. A., and Gellman, S. H. (2002) Analysis of the factors that stabilize a designed two-stranded antiparallel β-sheet. *Protein Sci. 11*, 1492−1505.
55. Snow, C. D., Qiu, L., Du, D., Gai, F., Hagen, S. J., and Pande, V. S. (2004) Trp zipper folding kinetics by molecular dynamics and temeprature-jump spectroscopy, *Proc. Natl. Acad. Sci. U.S.A. 101*, 4077−4082.
56. Grantcharova, V. P., Riddle, D. S., and Baker, D. (2000) Long-range order in the src SH3 folding transition state, *Proc. Natl. Acad. Sci. U.S.A. 97*, 7084−7089.
57. Klimov, D. K., and Thirumalai, D. (2002) Stiffness of the distal loop restricts the structural heterogeneity of the transition state ensemble in SH3 domains, *J. Mol. Biol. 315*, 721−737.
58. Klimov, D. K., Newfield, D., and Thirumalai, D. (2002) Simulations of β-hairpin folding confined to spherical pores using distributed computing, *Proc. Natl. Acad. Sci. U.S.A. 99*, 8019−8024.
59. Yang, W., and Gruebele, M. (2005) Kinetic equivalence of the heat and structural transitions of lambda {sub 6−85}, *Philos. Trans. R. Soc. London 363*, 565−73.

BI050698Z